Johnson Matthey's international journal of research exploring science and technology in industrial applications

∗∗∗∗∗∗∗∗∗∗∗∗Accepted Manuscript∗∗∗∗∗∗∗∗∗∗

This article is an accepted manuscript

It has been peer reviewed and accepted for publication but has not yet been copyedited, house styled, proofread or typeset. The final published version may contain differences as a result of the above procedures

It will be published in the **APRIL 2021** issue of the *Johnson Matthey Technology Review*

Please visit the website https://www.technology.matthey.com/ for Open Access to the article and the full issue once published

Critical Review of Earth-Abundant Borides and Phosphides for Water Electrolysis: Transition from the Lab to the Market

Alexey Serov

Pajarito Powder, LLC; Albuquerque, New Mexico 87109, USA

Kirill Kovnir

Department of Chemistry, Iowa State University, Ames, Iowa 50011, USA; Ames Laboratory, U.S. Department of Energy, Ames, Iowa 50011, USA

Michael Shatruk

Department of Chemistry and Biochemistry, Florida State University, Tallahassee, Florida 32306, USA; National High Magnetic Field Laboratory, Tallahassee, Florida 32310, USA

Yury V. Kolen'ko

International Iberian Nanotechnology Laboratory, Braga 4715-330, Portugal

Email: aserov@pajaritopowder.com, kovnir@iastate.edu, mshatruk@fsu.edu, yury.kolenko@inl.int

Abstract

To combat the global problem of CO_2 emissions, H_2 is the desired energy vector for the transition to environmentally benign fuel cell power. Water electrolysis (WE) is the major technology for sustainable H_2 production. Despite the use of renewable solar and wind power as sources of electricity, one of the main barriers for the widespread implementation of WE is the scarcity and high cost of platinum-group metals (PGMs) that are used to catalyze the cathodic hydrogen evolution reaction (HER) and the anodic oxygen evolution reaction (OER). Hence, the critical PGM-based catalysts must be replaced with more sustainable alternatives for WE technologies to become commercially viable. This critical review describes the state-of-the-art PGM-free materials used in the WE application. Several emerging classes of HER and OER catalysts are reviewed and detailed structure–property correlations are comprehensively summarized. The influence of the crystallographic and electronic structures, morphology, and bulk and surface chemistry of the catalysts on the activity towards OER and HER is discussed.

1. Sustainable H_2 generation by water electrolysis

Hydrogen is the first element of the Periodic Table and the most abundant element in the Universe. Currently, we are witnessing the emergence of H_2 gas as an increasingly powerful energy vector for storing/delivering electricity (1). Firstly, besides of having very low physical density, H_2 has highest gravimetric energy density of any known non-nuclear fuel (*e.g.*, three times higher than gasoline and 150 times higher than a state-of-the-art Li-ion battery), which sets the stage for H_2 as an efficient energy-storage solution (2). Secondly, H_2 is an environmentally benign fuel, since only energy and water are the end products of the reaction between H_2 and O_2, giving access to zero-emission electricity production when used in fuel cells. These benefits have made H_2 a priority area within the "climate and resource frontrunners" of the European Green Deal.

Currently, most of H_2 (ca. 95%) is produced through energy-demanding steam reforming reaction of water with natural fossils. Unfortunately, this translates into undesired generation of greenhouse gases. As an alternative, water electrolysis (WE), $2H_2O(l) \leftrightarrow 2H_2(g) + O_2(g)$, can be employed for H_2 production, providing a completely carbon-neutral solution when working on renewable electricity from wind, solar, wave/tide, biomass or geothermal, thus eliminating CO_2 emissions. Importantly, the resultant high-purity H_2 can be stored in a compressed or liquefied form or in chemical compounds (metal hydrides and liquid organic hydrogen carriers), and then delivered as needed for fueling small- and large-scale applications (3).

Although the era of WE began more than two centuries ago, its worldwide implementation is still limited to H_2 production up to the megawatt range using liquid alkaline electrolysis (4). WE is a kinetically controlled process characterized by slow charge transfer and insufficient chemical reaction rates. A large overpotential, defined as the difference between the required and thermodynamic value of the WE voltage [$E_0 = 1.23$ V *vs.* reference hydrogen electrode (RHE)], needs to be applied to drive this reaction. Therefore, catalysts, primarily based on platinum group metals (PGMs), are used to accelerate WE by reducing the value of the applied overpotential to conduct the cathodic hydrogen evolution reaction (HER) and the anodic oxygen evolution reaction (OER), which are the two half reactions of the WE (5).

The best-performing catalysts for WE are Pt for HER and IrO_2/RuO_2 for OER, featuring topmost activity and long-term stability in both acidic and alkaline electrolytes. Unfortunately, these PGMs are scarce and expensive, having the status of Critical Raw Materials in the EU. Ir/Ru are scarce even when compared to Pt because both are by-products of Pt mining. Hence, the use of PGMs has been recognized as one of the major bottlenecks for H_2 production by WE on TW scale, and, therefore, the development of PGM-free catalysts is an economically sound strategy towards technological and industrial expansion of the WE.

2. Membrane-based water electrolysis

On the electrolyzer side, the commercially available technologies for H_2 generation are based on (*i*) alkaline liquid electrolyzers (AELs), (*ii*) solid oxide electrolyzers (SOELs), and (*iii*) (semi)solid polymer electrolyzers (SPELs) (4, 6-9). The AEL technology has been commercially available for >50 years. It is characterized by long lifetime and low cost. The modern developments of AEL deal with the employment of high temperatures and pressures, targeting improvement of the efficiency (7). The AEL electrodes are typically composed of abundant Ni with a catalytic coating.

Shortcomings of the AEL are the use of corrosive liquid electrolytes (*e.g.*, KOH), low purity of the resultant H_2 due to high cross-permeation through cathode and anode separator, and long start-up times not suitable for dynamic operation. The currently developing SOEL (also known as steam electrolysis) omits the need for corrosive liquid electrolyte, but operates at temperatures above 700 °C, making the whole process energy demanding. Another issue is the instability and degradation of the electrode materials at the high operating temperatures. The WE technology based on SPEL is well-suited to intermittent supply applications at scale (dynamic operation), offering high current densities cf. AEL, high-purity H_2 at pressures up to 30 bar, and efficiency of ca. 70%. Nevertheless, a number of obstacles, such as high capital costs, prevent the widespread use of SPEL (9).

Advantageously, SPELs operate at low temperatures (50–80 °C), and the thin humidified polymer membranes feature high conductivity and low resistance, resulting in minimal current losses and low cross-permeation of H_2. There are three SPEL technologies: (*i*) proton-exchange membrane (PEM), (*ii*) anion-exchange membrane (AEM), and (*iii*) bipolar membrane (BPM).

PEM electrolyzers are the present state-of-the-art SPEL technology. Relatively compact PEMWE systems are available from several small, medium, and large companies, such as ITM Power, NEL, Giner, Enapter, Siemens, *etc*. Despite the fact that PEMWE has high Technology Readiness Level (TRL), it is still mainly used for demonstration projects, largely subsidized by local or national governmental funding organizations. The main reasons for the limited commercial adoption are high capital expenditures (CAPEX) and operational expenditures (OPEX), making the produced H_2 economically non-competitive cf. the traditional steam-reforming process.

More specifically, due to the extremely acidic protonic matrix of the ionomer and membrane (*e.g.*, Nafion, Aquivion, Celtec), the technology relies on scarce Pt/C and IrO_2/RuO_2 catalysts, which exhibit high intrinsic activity and durability (10). Notably, only these materials can withstand the acidic PEMWE operation conditions over a 20 year electrolyzer lifetime. Additionally, highly acidic and oxidative operation conditions dictate that the porous transport layers (PTLs) have to be made from corrosion-resistant but rather expensive Ti, which, combined with PGM catalysts, represents ca. 2/3 of the cost of the PEMWE stack (several individual PEM cells stacked together to achieve higher H_2 production).

The alternative AEMWE approach is rapidly growing from TRL2–3 to the level of TRL6–7 (11-13). AEM combines the advantages of AEL and SPEL, eliminating the need of corrosive liquid electrolyte and leveraging efficient membrane-based WE (14). Until recently, the main bottleneck in AEMWE was the lack of highly OH^- conductive, stable, and durable AEMs as compared to PEMs (15, 16). Fortunately, several promising AEMs have recently emerged on the market (17), such as those from Tokuyama, Fumatech, Ionomr, W7Energy, Ecolectro, Dioxide Materials, AGC, *etc*. The non-aggressive AEM environment at pH ≈ 13 and the possibility to produce AEMs without the use of fluorine (regulated in several countries) makes AEM production more environmentally friendly and safer for workers and nearby habitants (11).

Importantly, AEMWE may occur efficiently on PGM-free catalysts based on inexpensive metals (Fe, Co, Ni, *etc*.) that can also withstand prolonged operation in alkaline membrane environment. Therefore, the development of an electrolyzer based on emerging AEMs and PGM-free catalysts

should enable a significant reduction in both CAPEX and OPEX of the electrolysis (18). Interesting work on AEMWE within EU H2020 ANIONE project (https://anione.eu) additionally illustrates these points very well. Notably, a further CAPEX reduction can be achieved by replacing the expensive Ti PTLs by simple stainless steel, which is stable under AEMWE operation. Nevertheless, the detailed techno-economic analysis of AEMWE with PGM-free catalysts is complicated, and the projected cost of the as-produced H_2 strongly depends on the selected model and input parameters (19, 20).

A third, significantly less explored, avenue for SPEL is the BPM (21). Here, a PEM and an AEM are connected in series, thus allowing the use of non-Ir/Ru catalysts on the anode side. Notably, BPM provides a thermodynamic advantage due to the pH gradient across the membrane, which makes possible to conduct the electrolysis under applied potential below the standard potential of WE, thus requiring less current input. BPM technology is still in its infancy, and more research is required to improve its design, performance, stability, and cost.

Our research is focused on the development of PGM-free catalysts for alkaline HER/OER that could be further translated into real-life application of AEMWE. Various classes of PGM-free materials, such as alloys, (oxy)hydroxides, borides, carbides, nitrides, phosphides, chalcogenides, oxides, spinels, perovskites, MOFs, and metal-free C-based compounds, have been investigated as catalysts for alkaline WE. In this review, we will highlight several titled prospective PGM-free catalysts that have been studied in our laboratories.

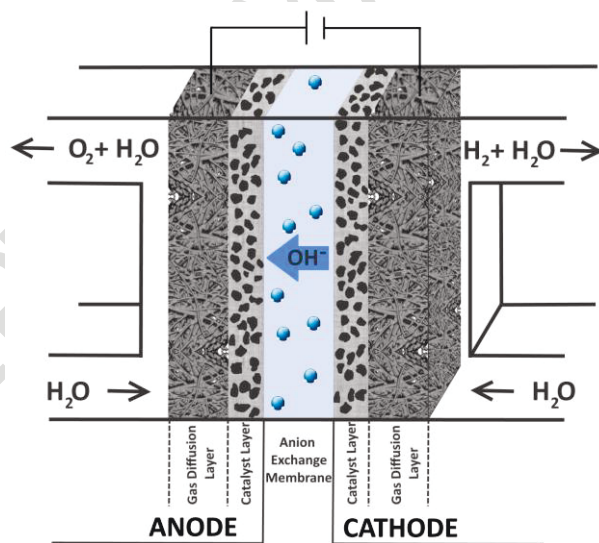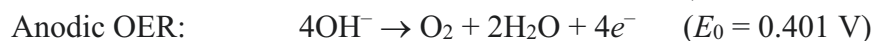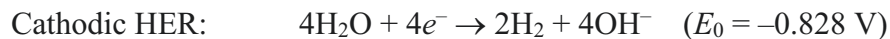## 3. Alkaline water electrolysis

Fig. 1. Schematic representation of a single AEMWE cell.

In the simple scheme of AEMWE cell (Fig. 1), the OER and HER catalyst layers are directly coated on the respective sides of the AEM membrane, thus forming a membrane electrode assembly (MEA). Alternatively, the catalysts can be incorporated into the respective gas-diffusion layer (GDL), thus forming a gas-diffusion electrode (GDE). Using porous GDLs is preferential *cf.* planar ones, since the porosity accelerates the mass transfer of the reactant/product over the

catalyst layer. The main role of the AEM is to ensure OH^- transfer from the cathodic side of the cell to the anodic side. Normally, AEM electrolyzers use a water feed with the addition of HCO_3^-/CO_3^{2-} or dilute KOH electrolytes to achieve better performance.

AEMWE allows for the direct generation of H_2 and O_2 through the following electrode reactions:

Cathodic HER: $4H_2O + 4e^- \rightarrow 2H_2 + 4OH^-$ ($E_0 = -0.828$ V)

Anodic OER: $4OH^- \rightarrow O_2 + 2H_2O + 4e^-$ ($E_0 = 0.401$ V)

Overall WE: $2H_2O \rightarrow 2H_2 + O_2$ ($E_0 = 1.229$ V)

As shown in Fig. 2a, HER starts with the electrochemical hydrogen adsorption $H_2O + M + e^- \leftrightarrow M–H^* + OH^-$ (Volmer reaction), where H* designates a hydrogen atom chemically adsorbed on an active site of the electrode surface (M). The initial adsorption can be followed by either electrochemical desorption, $M–H^* + H_2O + e^- \leftrightarrow M + OH^- + H_2$ (Heyrovsky reaction), or chemical desorption, $2M–H^* \leftrightarrow 2M + H_2$ (Tafel reaction). The exact mechanism and rate-determining step of the HER over certain catalyst can be established by the analysis of the respective Tafel slope data (22).
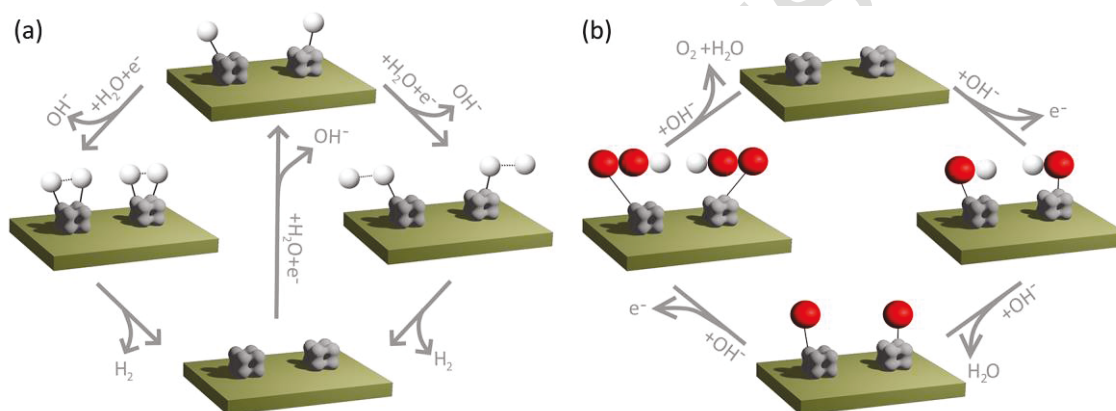

Fig. 2. Mechanistic Scenarios for the HER (a) and OER (b) in alkaline electrolyte.

The proposed alkaline OER (Fig. 2b) commences with the electrochemical adsorption of hydroxide anion on the electrode active site, $M + OH^- \leftrightarrow M–OH + e^-$, followed by the electrochemical formation of O- and OOH-bound intermediates: $M–OH + OH^- \leftrightarrow M–O + H_2O + e^-$ and $M–O + OH^- \leftrightarrow M–OOH + e^-$. Finally, O_2 molecule is generated as a result of the last single-electron charge-transfer step according to $M–OOH + OH^- \leftrightarrow M + O_2 + H_2O + e^-$. Notably, a scaling relation (23-26) between binding energies of the reaction intermediates results in a minimum theoretical, the so-called, "overpotential wall" of 0.37 V (27). This means that one would need to apply a minimum potential of 1.23 V + 0.37 V (*i.e.*, 1.6 V *vs.* RHE) to conduct the OER reaction, which has found experimental confirmation (28). Breaking the OER scaling relation and thus reducing/eliminating the "overpotential wall" still remains a challenge (29).

Table 1 summarizes parameters typically used to present laboratory half-cell data for the evaluation of the catalyst performance and comparison between different catalysts with similar mass loading per geometric area. A number of these parameters will be used in the subsequent discussion. The readers interested in the best practice for investigating novel HER and OER catalysts are referred to (30), while (31) provides useful guidance on analyzing and presenting the

catalytic data. Moreover, some critical aspects of electrochemical data evaluation are reported elsewhere (22, 32-34).

Table 1. Summary and explanation of parameters used to present laboratory half-cell WE data.

Parameter	Notation	Interpreted Properties or Behavior
Overpotential	η_j	The value of η at a defined current density, j (mA cm^{-2}), reflects catalyst activity
Current density	j	
Tafel slope	b	Reaction mechanism
Exchange current density	j_0	Intrinsic activity of the catalyst
Half-way potential	$E_{1/2}$	The potential required to achieve current that is half of the mass transport-limiting current density ($\frac{1}{2}j_{l,c}$)
Charge transfer resistance	R_{ct}	Charge transfer over catalyst/electrolyte interface
Geometric double-layer capacitance	C_{dl}	Electrochemically active surface area
Recorded data for cell electrolysis	$E(t) / j(t)$	Catalyst stability under galvanostatic/potentiostatic electrolysis conditions
Repetitive cyclic voltammetry	CV	Accelerated catalyst degradation
Faradaic efficiency	FE	Catalyst productivity towards target reaction. The ratio of the actual mass of a substance liberated from an electrolyte by the passage of current to the theoretical mass liberated according to Faraday's law

4. From precatalyst to catalyst during alkaline OER

OER, as a kinetically slow $4e^-$ transfer reaction, governs the overall efficiency of the WE. Since the largest overpotential stems from OER, catalyst development for this half reaction will offer the most efficiency gains (26).

Interestingly, initial reports employing transition metal borides, carbides, nitrides, phosphides, and chalcogenides (in general, Xides) as catalysts for alkaline OER putatively attributed the observed catalytic activity to the pristine materials. However, a careful consideration of following reasons indicated that all the aforementioned Xides should undergo oxidation during the OER into the respective oxides/(oxy)hydroxides (35):

(*i*) the alkaline OER is conducted under very oxidative conditions of pH $\geq$ 13, with the applied potential of $\approx$1.6 V *vs.* RHE;

(*ii*) the potential- and pH-dependent phase diagrams (Pourbaix diagrams) indicate existence of several oxo-containing phases for the corresponding metals under the conditions of alkaline OER;

(*iii*) the enthalpy of the formation of Xides is more positive than that of the respective transition metal oxides/(oxy)hydroxides.

Detailed characterization studies, including diffraction, spectroscopy, and microscopy analyses of the catalysts before and after alkaline OER, provided strong support for such an oxidation. Accordingly, all transition metal Xides could be considered as precatalysts or "active" supports for alkaline OER. The degree of oxidation could be different and largely controlled by the chemical nature of the Xide precatalysts. Moreover, the size and microstructure of the catalysts play an important role. If the catalyst nanoparticles (NPs) are ultrasmall or the active catalyst surface layer is very thin, the compounds will rapidly undergo full oxidation. In contrast, if the catalyst NPs/films are reasonably large/thick, then partial oxidation of the surface occurs, forming distinct core@shell NPs and nanoheterostructured films, preserving the bulk Xide structure underneath. In other words, in the case of poor catalysts, the oxidation of the bulk compound occurs forming non-conductive oxide/hydroxides, while for the good catalysts the oxide/hydroxide layer passivates the catalyst surface, preserving the bulk structure of the original compound.

The surface oxidation yielding the real catalyst is an unavoidable but crucial phenomenon to obtain highly active and stable OER catalysts. In the vast majority of studies, the resultant *in situ* formed catalysts show remarkably higher OER performance than their respective metal oxide/hydroxide counterparts. Full understanding of this performance enhancement is still lacking. Generally, there are several factors that should be pointed out: (*i*) the development of high surface area due to the formation of amorphous-like (oxy)hydroxide surface, (*ii*) the high conductivity of the non-oxide Xide precatalyst underneath the real catalyst, and (*iii*) synergetic catalyst–precatalyst electronic interactions within the as-formed nanoheterointerface (35-37). These factors give rise to a larger number of catalytically active sites and faster charge transfer kinetics over the anode/electrolyte interface, thus beneficially boosting the OER performance.

Currently, there is a limited knowledge of the mechanism of surface transformation during OER because mainly *ex situ* studies are performed before and after OER. *In situ* surface-sensitive studies (such as spectroscopy, diffraction, imaging, electrochemical imaging, cyclic voltammetry, nanoimpacts, and combination thereof), despite being extremely challenging, are crucial for the rational development of the OER precatalysts (38-42). Such knowledge will be essential to achieve control over the formation of the real catalyst, thus guiding our future efforts towards active, stable, and economic catalysts for alkaline OER (Fig. 3).

To summarize, the structure of the bulk phase or core of NPs of a prominent OER catalysts is preserved during the reaction. The surface is, undoubtedly, oxidized due to the extreme oxidation potential applied and the presence of multiple active species, such as hydroxide radicals. The formed oxide layer passivates the surface, thus preventing further oxidation of the bulk of the precatalyst. The same oxide layer is an active catalyst. Thus, the formation of the oxide layer should not be avoided but rather judiciously directed to enhance stability and activity of the catalysts. A combination of computational and detailed *in situ* studies is a promising strategy in this research direction.
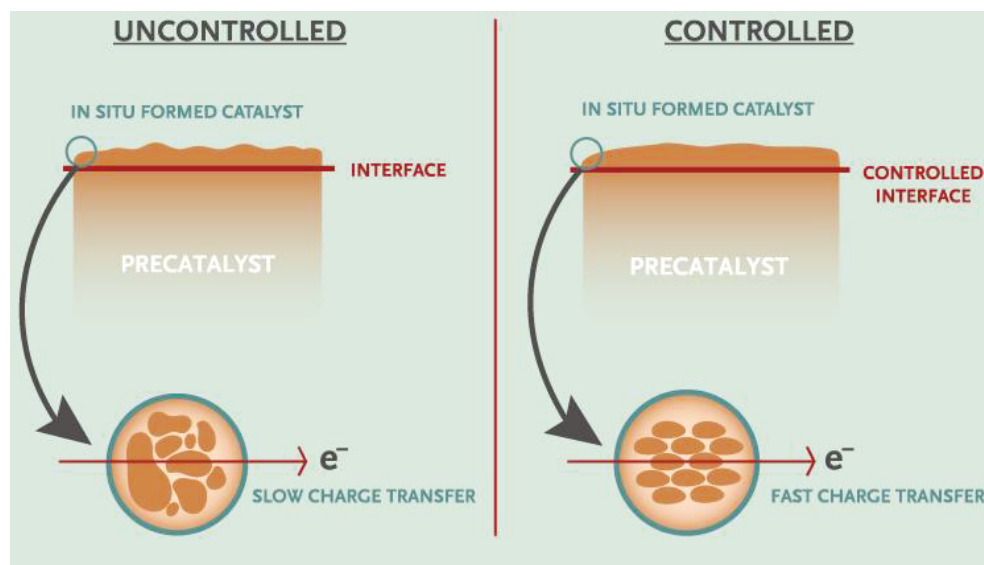
Fig. 3. Interface engineering approach toward new catalysts for OER.

5. Current industrially-relevant PGM-free catalysts for alkaline HER/OER

Thorough and comprehensive studies conducted by research groups around the globe have narrowed down the range of industrially-relevant PGM-free HER/OER catalysts for AEMWE to (*i*) Ni, Ni alloys, and intermetallic compounds as the most active and stable for the HER side of the MEA (43-51) and (*ii*) base metal oxides, (oxy)hydroxides, spinels, and perovskites for the OER side of the MEA (52-58).

In general, the catalysts for alkaline HER are similar to those used in the AEM fuel cells (AEMFC) (59). C-supported Ni, Ni–Mo, Ni–Cu, and other Ni-based catalysts have been synthesized and investigated (43-51). As a lighter analogue of PGMs (especially being chemically similar to Pd), Ni plays the main role in HER, while the addition of other elements increases the cathode durability. Ni–Mo catalysts have been intensively studied for both hydrogen oxidation reaction and HER under realistic AEMFC and AEMWE conditions, respectively (45, 48, 50). The Ni–Mo alloys enriched with Ni up to ≈87 at.% were found to be not only active in alkaline HER, but also less prone to poisoning by functional groups of ionomers, which is a well-known shortcoming of PGM catalysts in AEMFC and AEMWE (45, 48). The properties of C supports, such as the surface area, level of graphitization, bulk/surface chemical composition, and hydrophobic/hydrophilic properties, significantly affect the AEMWE performance and should be carefully tuned as a function of the type, composition, and weight loading of the HER catalysts (60).

Considering the OER catalysts, Ni (oxy)hydroxides/oxides with Fe impurities in alkaline electrolyte, as well as the NiFe (oxy)hydroxides, have become benchmark catalysts for AEMWE (61, 62). Although the exact nature of the active catalytic sites in such systems is not well understood (63), the NiFe-based materials for alkaline OER deserve a more careful study in the future, especially with respect to their low durability issues (64, 65).

Furthermore, a general direction in the development of the catalysts for alkaline OER is to improve the electronic conductivity of already established active oxide catalysts, since the conductivity of

the oxides is typically very low. Such an improvement is critical to reducing the applied overpotential during the real AEMWE operation, where loading of OER catalysts can often be as high as 4–12 mg cm^{-2} (53-55). Unfortunately, the oxidative operation conditions during OER at high potential of ≈1.9–2 V forbid the utilization of traditional highly conductive C supports, which would simply oxidize and degrade during prolonged AEMWE. At the same time, using C as a supporting material for transition metal oxide catalysts is a common laboratory practice in short half-cell experiments for the initial assessment of intrinsic catalytic activity of the materials and performance losses due to insufficient electronic conductivity (52). For instance, highly graphitic C nanotubes or high surface area graphenes are widely used during the screening and selection of promising alkaline OER materials (12, 52). An alternative strategy is based on employing non-stoichiometric mixed oxides, perovskites, delafossites, or spinels (58). Although these materials possess high conductivity (> 0.1 Ω^{-1} m^{-1}) (58), specific synthetic methods should be developed to produce such conductive oxides on a large scale.

Notably, the commercial metal oxide products made on the multi-ton scale are mainly silica, zeolites and titanium dioxide. The protocols used to manufacture these materials are well-matured and based on the sol-gel, precipitation, hydrothermal, flame or spray pyrolysis. Nevertheless, these approaches have a limited ability to control physico-chemical properties required for OER catalysts, including phase purity (required for high electronic conductivity), the surface area (required for higher density of active sites), the primary particle size (required for the uniform distribution in the electrode structure), *etc*.
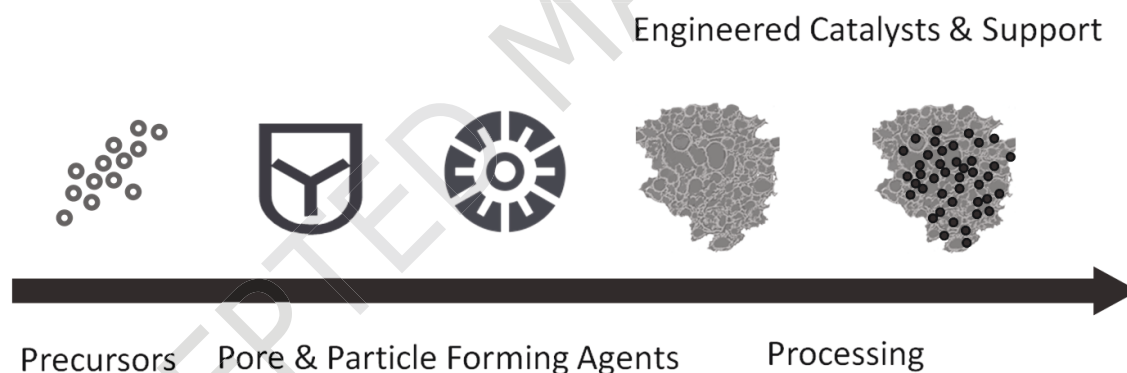

Fig. 4. Schematic representation of VariPore™ method for the mass production of PGM-free HER/OER catalysts.

For the last 8 years Pajarito Powder (https://pajaritopowder.com) re-designed and modified their proprietary manufacturing platform VariPore™ for upscaling mixed oxide catalysts production. The schematic of the method is shown on Fig. 4. The main idea of this method is designing material by the bottom-up approach with the ability to control all required properties of final catalyst at every stage of the process. For example, selecting particle and pore forming agents (P&PAs) with different morphology will afford a final catalyst with an inverted structure of the respective P&PAs. The chemical nature of the precursors will allow selection of manufacturing conditions to

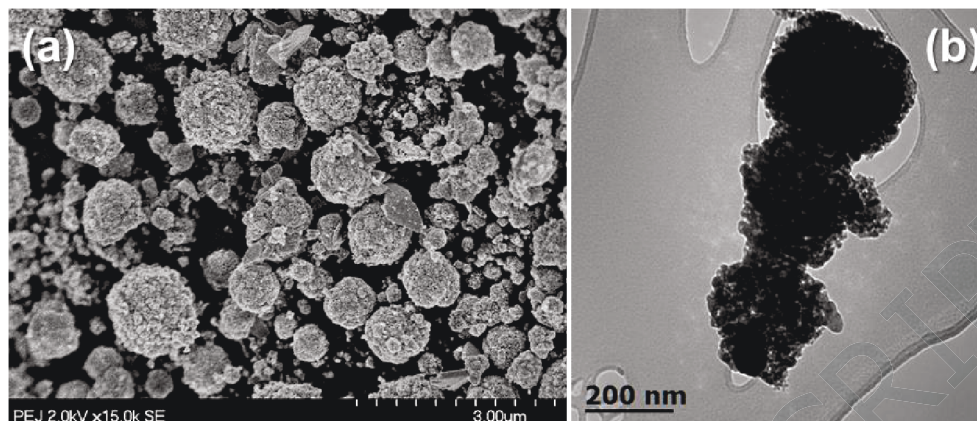obtain materials under low energy demanding regime, substantially decreasing the cost of final materials.

Fig. 5. SEM (a) and TEM (b) images of $CuCo_2O_4$ catalysts prepared by scalable approach (58).

The method was successfully used for the preparation of phase-pure $CuCo_2O_4$ spinel catalyst for OER (Fig. 5a). The P&PAs used in this design derived from high surface area spherical silica particles, which prevented NPs from agglomeration. The phase purity of the spinel was achieved by thermal treatment at just 550 °C, allowing to preserve the unique spherical shape of agglomerates (Fig. 5b). The latter is important for manufacturing the dense electrodes for OER, allowing maximal catalyst utilization on the GDEs. At the moment, this method is established as a robust, flexible and modular manufacturing platform for making different classes of HER/OER catalysts and practiced for commercial production at the kg scale per batch (54).

Among the large variety of PGM-free catalysts that are currently extensively explored, the interest of our groups have been focused on transition metal phosphides and borides, which belong to a larger family of non-oxide catalysts referred to as Xides. In the next two sections, we focus specifically on these two groups of Xides, highlighting some of our results along with important findings from other research groups. For a more general overview of PGM-free non-oxide electrocatalysts, we refer the reader to several recent reviews relevant to this topic (36, 66, 67).

6. Emerging transition metal phosphide catalysts

6.1 Crystal and electronic structure

Transition metal phosphides (TMPs) are considered promising alternatives to PGM catalysts for WE. Phosphides of earth-abundant transition metals, Fe, Co, Ni, and Mo, are mainly studied with stoichiometries ranging from M_2P to MP_2. The crystal structures of TMPs are quite different from the structures of the corresponding metals. In the crystal structures of phosphorus-rich MP and MP_2, each M atom is surrounded by six or seven P atoms forming P_6 octahedra (Fe, Co, Ni), P_6 trigonal prisms (MoP), or P_7 monocapped trigonal prisms (MoP_2) centered by M atoms. The coordination of M atoms in metal-rich M_2P phosphides is composed of four or five P atoms forming tetrahedra or square pyramids around the M atoms (Fig. 6).
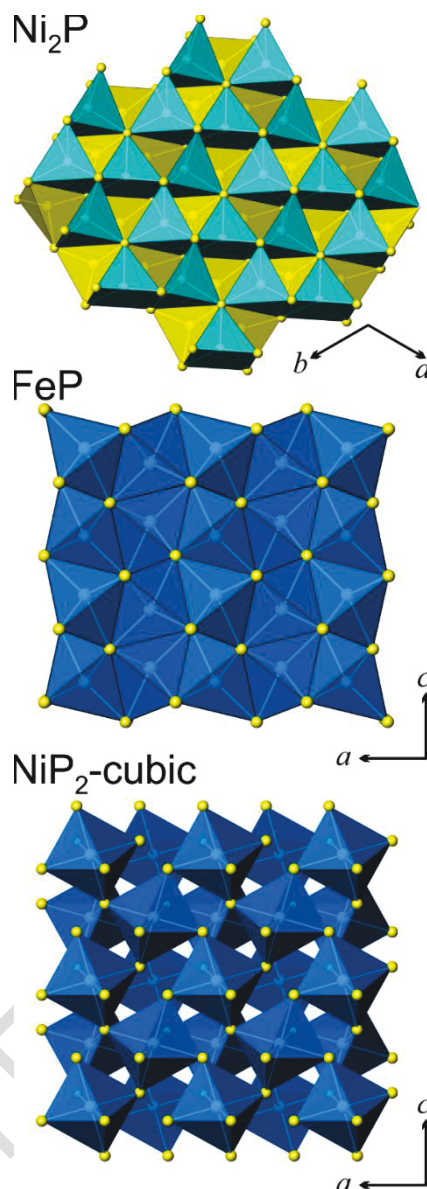
Fig. 6. Crystal structures of selected phosphides. *M*: white, P: yellow. NiP_4 tetrahedra: yellow; NiP_5 square pyramids: cyan; FeP_6 and NiP_6 octahedra: blue.

In all TMPs, strong covalent bonds between P and *M* atoms are formed due to substantial overlap of *M*–3*d* / *M*–4*s* and P–3*p* orbitals, resulting in significant changes in the electronic structure and chemical properties as compared to elemental metals. These changes lead to the higher chemical stability of TMPs under HER/OER conditions cf. elemental Fe, Co, Ni, and Mo metals. The majority of the studied phosphides have metallic properties with non-zero density of states (DOS) at the Fermi level (E_F). Fe, Co, and Ni phosphides with identical composition are either isostructural or closely structurally related, which allows fine tuning of the Fermi level positions, as illustrated in Fig. 7 for the example of M_2P compounds. FeP, CoP, and MoP also exhibit metallic properties. In the case of Ni phosphides, NiP is a high-pressure phase while at ambient conditions one obtains Ni_5P_4, a stable metallic phosphide with excellent catalytic properties. Further increasing the P content in TMPs results in semimetallic properties for MoP_2 and narrow-bandgap

semiconducting properties for MP$_2$ with M = Fe and Co, and Ni. Again, Ni is a special element due to the existence of a cubic metallic polymorph NiP$_2$. This compound was originally assumed to be a high-pressure phase but was shown to be a metastable polymorph that can be synthesized at ambient pressures (68).
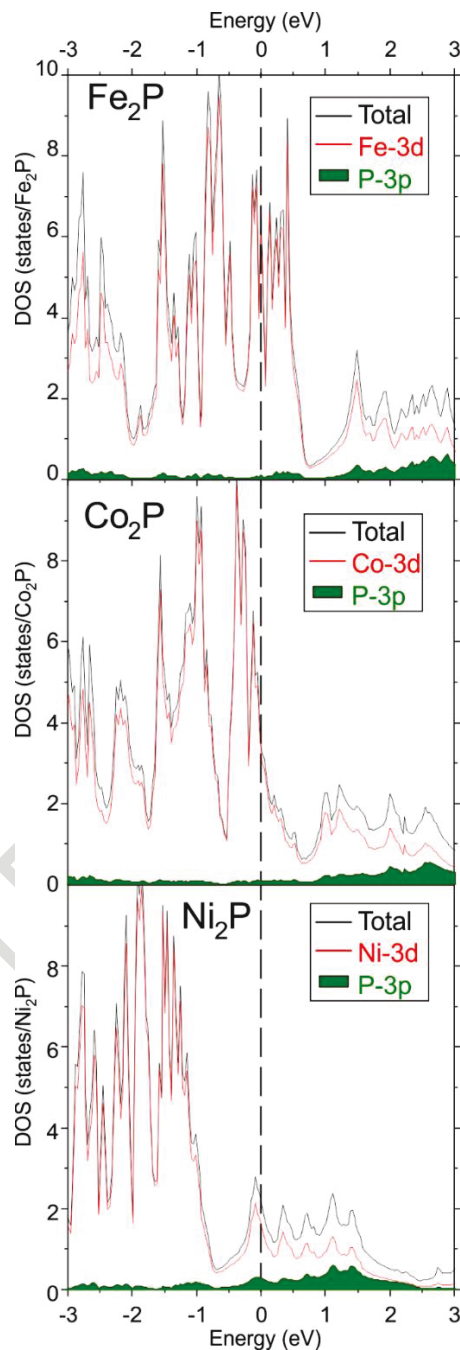

Fig. 7. DOS normalized to M_2P formula unit for Fe, Co, and Ni phosphides. The red line shows the dominant contribution of M–$3d$ states while the P–$3p$ contribution is highlighted in green.

6.2 HER catalysis

Currently, several hundred research papers describing TMP catalysts for HER and OER are published annually (37, 69, 70). Despite the large number of studies, there are two issues in this field: (*i*) the reported data are very scattered in terms of performance, and (*ii*) very few attempts have been reported that go beyond half-cell measurements in the research laboratory by making an actual electrolyzer using TMPs. The former issue is illustrated in Fig. 8, which shows the data published for the HER performance of CoP catalysts in acidic media. Although in all cases the material is reported to be single phase CoP, mainly in the form of NPs, the performance is quite scattered. While certain variability in the data is due to different setups, testing protocols and sample preparation routines used in various labs, the reported CoP NPs have different shapes, crystal facets exposed, surface termination by ligands, and surface area, thus making the analysis of the reported data non-trivial.
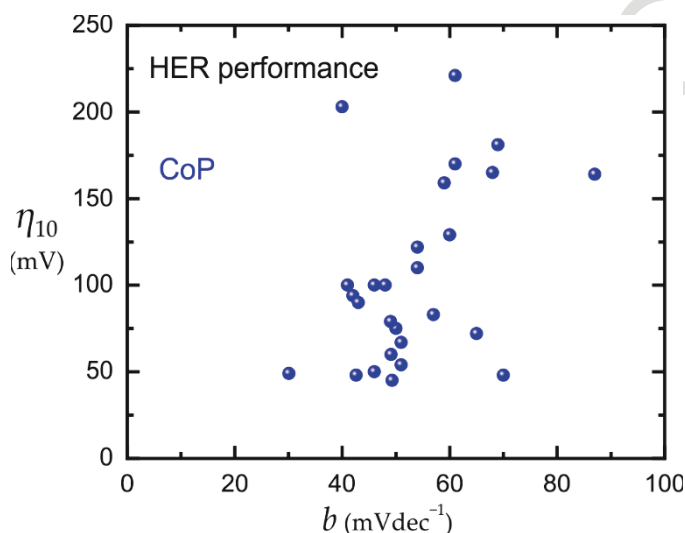

Fig. 8. Tafel slopes (*b*) and overpotentials required for driving current densities of 10 mA cm^{-2} (η_{10}) for the selected examples of acidic (0.5 M H$_2$SO$_4$) CoP HER catalysts (69).

The Kovnir and Kolen'ko groups have been exploring TMPs as an alternative to PGMs in WE since 2014, partially through EU H2020 CritCat project (http://www.critcat.eu), with significant progress in understanding the limitations and potential of new PGM-free catalysts (69). A Ni–P material was synthesized by gas-transport phosphorization of commercial Ni foam (71). The resultant self-supported foam cathode was highly active toward acidic/alkaline HER in terms of overpotentials, exchange current densities, and Tafel slopes (71). To reduce the mass loading of the Ni–P catalyst in the foam cathode (60 mg cm^{-2}), a thin-film Fe$_{0.2}$Ni$_{0.8}$P$_2$ supported on C paper was prepared through combination of sputtering and gas-transport phosphorization. The material demonstrated excellent acid/alkaline HER performance with only 1 mg cm^{-2} catalyst mass density (72).

Notably, surface characterization of TMPs during reaction is quite limited. In the vast majority of cases, the surfaces are characterized before and after the reaction. X-ray photoelectron spectroscopy (XPS) and related spectroscopic techniques often reveal significant presence of oxides on the surface of the used catalysts. This observation has led to a common suggestion that

the surface of the TMP catalysts is restructured/oxidized during the HER. An open question remains whether this assumption is true and how the bulk crystal structure of the phosphide impacts its catalytic properties. A recent study of two polymorphs of NiP_2 shows that the bulk structure has a significant impact on the catalytic properties of the corresponding phosphide (68). One possible explanation is that the monoclinic polymorph of NiP_2 is a semiconductor, while the cubic one has metallic properties, which might be sufficient to explain the observed difference in reactivity instead of their bulk crystal structures.

A recent study on single crystals of FeP and monoclinic NiP_2 has shown that different facets of the same crystal exhibit different catalytic activities (73). Moreover, the activity was demonstrated to correlate with the computed surface H adsorption energy on the P atoms of the corresponding facet. This finding clearly highlights that both the underlying bulk structure and the specific surface termination play an important role in the performance of HER catalysts. Formation of surface oxides may be explained by oxidation of P–H bonds upon exposure of used catalysts to ambient conditions.

In contrast to hundreds of papers reporting fascinating properties of various TMPs, very few TMPs were tested beyond simple HER half-cell measurements in solution. To the best of our knowledge, there are only few reports, – one for each metal phosphide, NiP_2, CoP, FeP, and MoP, – of assembling a complete PEMWE single cell using TMPs as cathodes and Ir or Ir/Ru oxides as anodes (74). An interesting example of achieving a current density of 0.88 A cm^{-2} at applied potential of 2 V with CoP NPs as HER catalyst in a commercial-scale 86 cm^2 PEMWE was reported by King and co-workers (75). Further, it has been shown that for cubic NiP_2 only a 13% increase in potential was required in gas-phase PEMWE operation to achieve a current density of 50 mA cm^{-2} as compared to Pt electrode [1.86 V for cubic NiP_2 *vs.* 1.64 V for Pt] (68). Very recently, a cathode of highly crystalline FeP NPs supported on commercial conductive C was used to achieve a current density of 200 mA cm^{-2} at 2.06 V cell compared to 1.71 V with reference Pt cathode, corresponding to a difference of only 0.07 W cm^{-2} in the power input (74). Separate experiments showed up to 100 h of cathode operation in PEMWE, as well as stable switch-on and shut-down cycle dynamic operation during 36 h. Importantly, our NiP_2 and FeP catalysts show PEMWE HER performance on par with the best reported Pt-free materials (75-77).

6.3 Alkaline OER catalysis

While for HER Pt has not been beaten, TMPs excel at alkaline OER, outperforming simple reference Ir and Ru oxide catalysts. Table 2 provides several examples of TMPs studied as OER electrocatalysts, summarizing their performance characteristics and the conditions used for the catalyst synthesis. The surface chemistry of TMPs under OER conditions is more complex than that for HER. As discussed in *Section 4*, under OER conditions the top surface layers of phosphides undergo oxidation while the bulk material remains intact. The active catalyst is thus an oxygen-containing phase, which can be any combination of transition metal oxide, hydroxide, and phosphate. In the best-performing OER TMP catalysts, this oxidized layer is relatively thin and coherently interfaced to the underlying metal phosphide bulk. The formed heterostructure is crucial for high performance because simple catalysts composed of transition metal oxides/hydroxides show much lower activity. The role of TMPs is to serve as precatalyst to template thin *in situ*

oxidized active surface layer and efficiently supply current to this layer through the bulk conductivity of the TMPs (37).

At the same time, the importance of the bulk structure of TMPs for OER catalysis can be demonstrated in our comparative study of two polymorphs of NiP_2 (68). Cubic NiP_2 is a metallic conductor, while monoclinic NiP_2 is a semiconductor. During the OER reaction both polymorphs are expected to oxidize to a similar surface phase because of identical composition. However, the OER performance of the polymorphs was different (Table 2), emphasizing that the bulk structure of the TMP OER catalysts is an important factor determining the catalyst activity.

Interestingly, the aforementioned $Fe_{0.2}Ni_{0.8}P_2$ catalyzes the OER in alkaline media as well, showing reasonably high activity (Table 2). More importantly, $Fe_{0.2}Ni_{0.8}P_2$ serves as precatalyst for the *in situ* generation of the active catalyst during water oxidation. Since the $Fe_{0.2}Ni_{0.8}P_2$ catalyst film was quite thin, it underwent complete oxidation during OER into amorphous-like Fe-containing $Ni(OH)_2$, which remained active and stable for at least 60 h of alkaline OER. Based on the concept of *in situ* formation of real catalysts, the activity and stability of this system was further improved by interfacing the Ni_2P NP precatalyst with Mg oxyhydroxides (78). In contrast to the complete oxidation of $Fe_{0.2}Ni_{0.8}P_2$ observed in the previous study, it was found that Ni_2P NPs form distinct core−shell structures during alkaline OER (Fig. 9), and the resultant catalyst shows η_{10} of only 280 mV (Table 2), while being stable over 8 days.

Table 2. Selected examples of alkaline OER performance for TMP catalysts.

Compound	η_{10}, mV	b, mV dec^{-1}	Synthesis[a]	Ref.
RuO$_2$	310	$\approx$70	commercial source	(79)
IrO$_2$	320	$\approx$90	commercial source	(79)
Cubic NiP$_2$	340	56	NiCl$_2$ + P, 40 h at 773 K; H$_2$O; ball-milling	(68)
Monoclinic NiP$_2$	410	61	Ni + P, 76 h at 973 K; ball-milling	(68)
Cubic Fe$_{0.2}$Ni$_{0.8}$P$_2$	140	49	Fe$_{0.2}$Ni$_{0.8}$/C paper + P, 1 h at 773 K, 12 h at 523 K	(72)
Ni$_2$P	310	48	Ni/C paper + P, 6 h at 773 K	(78)
Mg-modified Ni$_2$P	280	71	Ni/Mg/C paper + P, 6 h at 773 K	(78)
Ni$_5$P$_4$-Ni$_2$P	250	54	Ni foam + P, 2 h at 873 K	(79)
Al-modified Ni$_5$P$_4$-Ni$_2$P	180	27	Ni foam/Al + P, 2 h at 873 K	(79)

[a] Sequential synthetic steps are separated by semicolons. See the cited articles for detailed synthetic procedures.
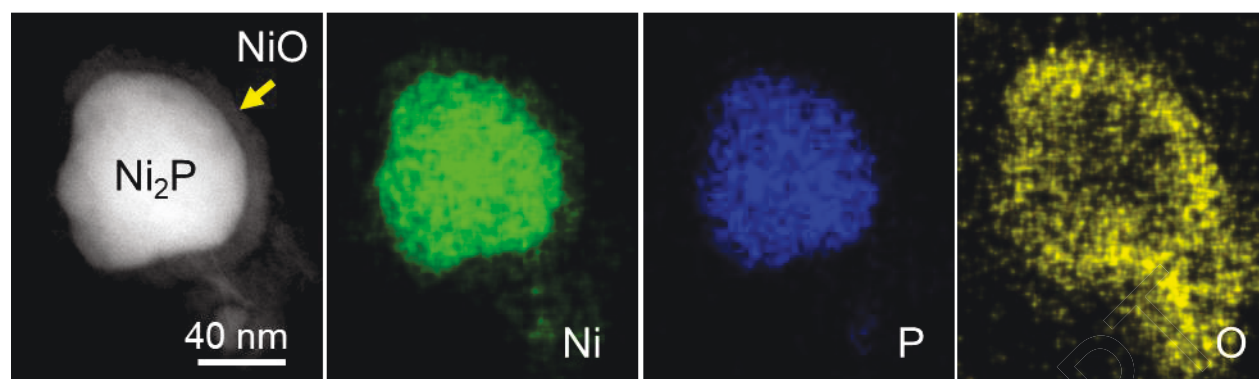
Fig. 9. HAADF−STEM image showing the development of Ni₂P@NiO nanostructure after catalytic testing of Ni₂P NPs in alkaline OER, together with the EDX maps of Ni, P, and O (78).

A self-supported Al-doped Ni–P foam cathode has been recently developed as a highly active material for HER. The substitution of Al for Ni atoms in the crystal structure of Ni phosphide favorably modifies the electronic structure of the resultant cathode (80). The knowledge that Al dissolves in KOH (similar to selective etching of Al from Al–Ni alloys to form Raney Ni catalyst) and the catalyst is formed *in situ* from the Ni–P precatalyst has led to implementation of a foam anode with good physical mixing of Al and Ni–P at the foam surface (79), in contrast to the chemical doping above. Sacrificial leaching of the Al phase coupled to the oxidation of the Ni–P precatalyst produced a high-surface area real catalyst exhibiting an impressive Tafel slope of 27 mV dec^{-1} and offering anodic current densities of 10, 100, and 300 mA cm^{-1} at overpotentials of merely 180, 247, and 312 mV, respectively (Table 2). In addition, the anode demonstrated an excellent stability during galvanostatic electrolysis, providing steady $j = 10$ mA cm^{-2} at very low $\eta \approx 185$ mV for over 8 days. This is one of the best-performing PGM-free anodes reported for alkaline OER (79), marking that Al scaffolding plus *in situ* precatalyst oxidation has unprecedented potential towards alkaline OER anodes (81).

7. Emerging transition metal boride catalysts

7.1 Crystal and electronic structure

Transition metal borides (TMBs) represent another appealing group of Xides for WE. Similar to phosphides, borides of various stoichiometries are known for the majority of transitions metals, including the earth-abundant Fe, Co, and Ni. A distinct characteristic of TMBs is the relatively small size and electron-deficient nature of boron atoms, which result in dense crystal packing and extensive contacts between metal atoms (82), even in the structures with a relatively high boron content (*e.g.*, *M*B). Therefore, in contrast to TMPs, a more appropriate way to describe TMB structures with more than 50 at.% of *M* is to consider boron-centered polyhedra of metal atoms.

Representative TMB structures are provided by iron borides, Fe₃B, Fe₂B, FeB, and FeB₂. As one traverses this series, the Fe–B distances remain consistent within the range from 1.95 to 2.35 Å, while each B atom becomes surrounded by fewer Fe atoms and the B–B bonding becomes more extensive (Fig. 10). The structure of Fe₃B is assembled of tricapped trigonal prisms, Fe₉B, that fill up the volume by edge-sharing. The nearest B–B distance is 3.24 Å, suggesting the lack of any bonding between B atoms. In Fe₂B, each B atoms is enclosed in a bicapped trigonal prism of Fe

atoms that can be also described as a flattened square antiprism. The antiprisms share basal faces that are perpendicular to the c axis of the tetragonal lattice, resulting in short B–B distances of 2.13 Å along that direction. Thus, linear chains of B atoms are observed along the c axis. The crystal packing is completed by the antiprisms sharing edges in the ab plane. Even shorter B–B distances, 1.79 Å, are found along zigzag chains observed in the FeB structure, where each B atom is surrounded by only seven Fe atoms that form a monocapped trigonal prism. Finally, a substantial change is observed in the structure of FeB_2, where Fe atoms are sandwiched between honeycomb layers of B atoms, which can be considered isoelectronic to graphene if the oxidation state of +2 is assigned to Fe while the coordination environment of Fe is reminiscent of the ferrocene molecule. The B–B distance in the layer is 1.76 Å, only slightly shorter than the distance observed in the zigzag chains of B atoms in FeB.

Other TMBs exhibit structures similar to those of iron borides. It should be also mentioned that Fe_3B, Fe_2B, and FeB_2 are representatives of the structure types of Fe_3C (cementite), Al_2Cu, and AlB_2, respectively, while FeB is the parent of its own structure type.
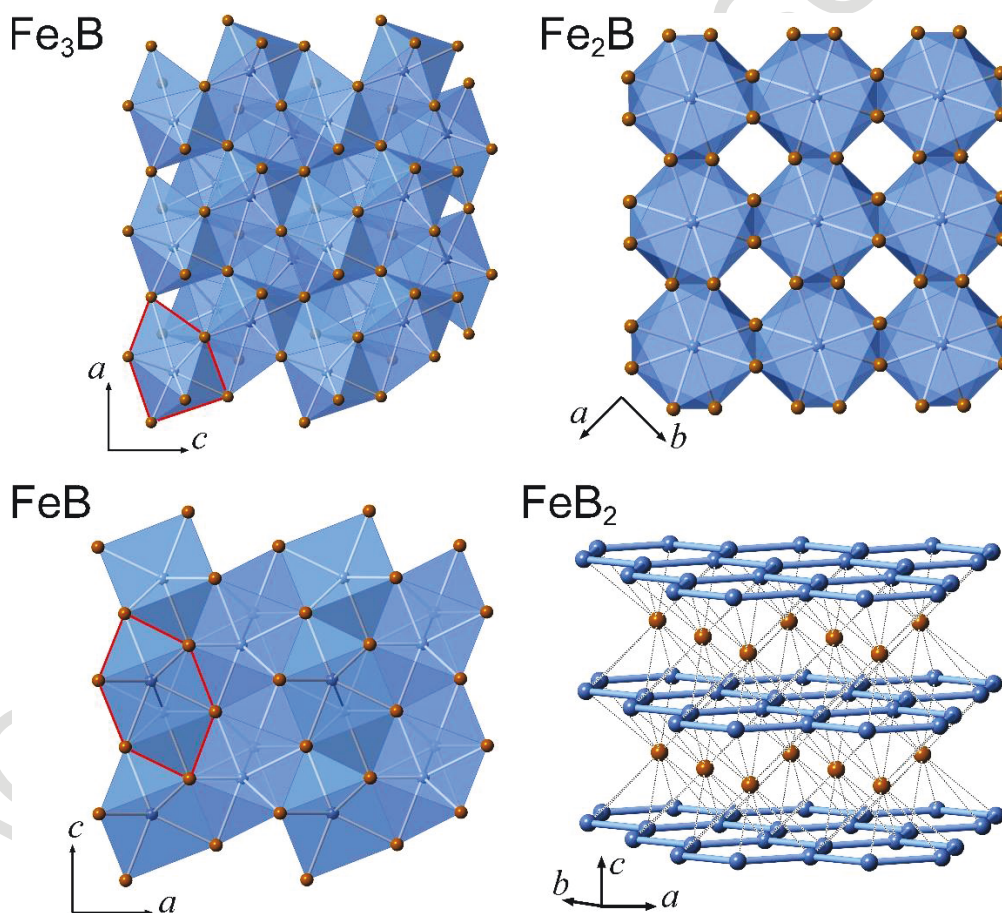

Fig. 10. Crystal structures of selected iron borides. Fe: brown, B: blue. The tricapped trigonal prisms BFe_9 in the structure of Fe_3B and the B–B bonded chains of monocapped trigonal prisms BFe_7 in the structure of FeB are emphasized with red contours. The structure of FeB_2 emphasizes the honeycomb layers of B atoms that sandwich 12-coordinate Fe atoms.

Due to the smaller size of B atoms, extensive $M–M$ contacts permeate the crystal structures of metal-rich TMBs (M_xB_y with $x/y \geq 1$). As a result, the electronic structures of these materials feature non-zero DOS at the E_F, resulting in metallic behavior. High electrical conductivity can be beneficial when TMBs are used as catalysts or precatalysts for electrochemical reactions that afford rapid transport of electrons between the external circuit and the catalyst-electrolyte interface. Moreover, the substantial hybridization of $3d$ orbitals in borides of first transition row metals leads to appearance of pronounced DOS peaks in the electronic structure. When the E_F is tuned to cross these peaks, the resulting electronic instability is resolved by spontaneous spin polarization that manifests itself as magnetic ordering in the macroscopic response of the material (83). For example, metallic Ni$_3$B can be tuned into ferromagnetic behavior by partial substitution of Co for Ni, which lowers the electron count in the system, changing the position of the E_F with respect to the DOS features (Fig. 11). The predictability of such changes is facilitated by the isostructural nature of $3d$ metal borides with specific compositions. A strong magnetic response may be beneficial for improving the efficiency of WE in the presence of an applied magnetic field, as has been shown in several recent reports (84-87).
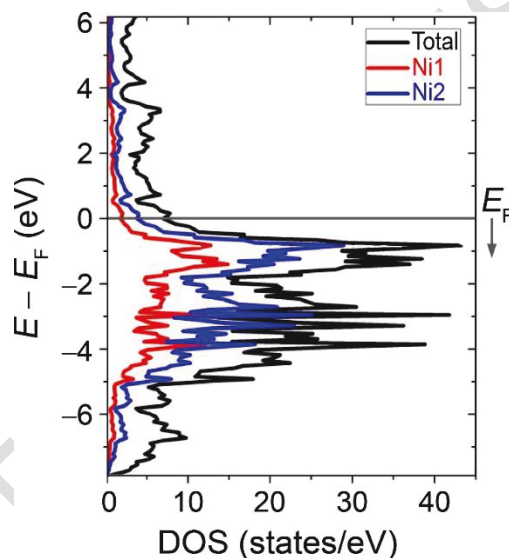

Fig. 11. DOS of Ni$_3$B showing the high peak positioned below the E_F. The arrow indicates the direction in which the E_F will be shifted due to substitution of Co for Ni.

7.2 HER catalysis

Similar to TMPs, the substantial hybridization between the metal d orbitals and boron p orbitals results in strong covalent $M–B$ bonding in TMBs. As a result, the free energy of H atom absorption is lowered in comparison to pure metal catalysts, and such TMBs as RuB$_2$ (88), MoB$_2$ (89), FeB$_2$ (90), and VB$_2$ (91) exhibit high HER activity in both acids and bases. In fact, RuB$_2$ shows activity similar to that of Pt metal under acidic conditions and outperforms Pt under alkali conditions (92). Besides the higher catalytic activity, RuB$_2$ was also shown to be more acid- and base-resistant as compared to borides with higher Ru content. Lower activities in HER have been observed for other metal-rich TMBs, *e.g.*, MoB (93) and Mo$_2$B (94), and Fe$_2$B (95). Yet again, similar to TMPs, the majority of studies on the catalytic properties of TMBs have been limited to the half-cell HER measurements (Table 3). A notable exception is the study of the overall water splitting in an

alkaline electrolyzer utilizing FeB_2, which achieved the current density of 10 mA cm^{-2} at 1.57 V (90), comparable to the state-of-the art systems.

An interesting approach to modifying the catalyst structure was suggested by Schaak and co-workers, who studied the HER catalyzed by AlMoB (96). The structure of this material can be obtained by inserting layers of Al atoms into the FeB-type structure discussed above (Fig. 10). This spatial separation of the [MoB] layers is expected to enhance their catalytic activity. The HER at pH = 0 proceeded with a rather high overpotential, η_{10} = 400 mV. To increase the access to the catalytic sites, the authors soaked the material in NaOH, which led to partial removal of Al. After treatment with acid, to decrease the concentration of OH-terminated sites, the overpotential η_{10} recorded at pH = 0 decreased to 301 mV. These findings suggest that the spatial separation of the catalytically active blocks by insertion of other structural fragments might be a viable strategy toward enhancing the catalytic activity of Xides, in general.

Table 3. Selected examples of HER performance for TMB catalysts.

Compound	pH	η_{10}, mV	b, mV dec^{-1}	Synthesis[a]	Ref.
RuB_2	0	16	30	K_2RuCl_5 + MgB_2, 3–10 h at 973–1223 K; 0.5 M H_2SO_4; H_2O/ethanol	(88)
RuB_2	14	25	28	K_2RuCl_5 + MgB_2, 3–10 h at 973–1223 K; 0.5 M H_2SO_4; H_2O/ethanol	(88)
FeB_2	14	61	88	$FeCl_2$ + $LiBH_4$ in THF, 2 h at reflux; centrifugation; H_2O; 2 h at 873 K	(90)
MoB_2	0	149	76	Mo + B, 15 min at 2073 K and 5.2 GPa	(89)
VB_2	0	192	68	VCl_3 + B + Sn, 8 h at 1073 K; 10% HCl; H_2O/ethanol	(91)
MoB	0	212	55	commercial source	(93)
MoB	14	220	59	commercial source	(93)
AlMoB	0	301	–	Al(excess) + Mo + B, 10 h at 1673 K; 3 M HCl; H_2O	(96)
Mo_2B	0	>400	128	Mo + B, arc-melting; manual grinding	(94)

[a] Sequential synthetic steps are separated by semicolons. See the cited articles for detailed synthetic procedures.

7.3 Alkaline OER catalysis

Recently, TMBs have been shown to exhibit excellent electrocatalytic activity toward OER under alkaline conditions. As emphasized in the *Section 4*, the nature of OER leads to complex chemical processes that result in inevitable surface oxidation of the catalyst. Thus, the works that attribute the OER activity to intrinsic behavior of TMBs should be taken with a grain of salt. Careful studies of these reactions confirm the formation of a shell of catalytically active oxides and hydroxide NPs

around the core TMB structure, which, therefore, should be described as a precatalyst. The role of the precatalyst is similar to that already discussed for the case of TMPs: it provides the structural support to the *in situ* form oxidized surface shell and also facilitates electron transport between the catalytically active surface and the external circuit.

In contrast to HER, where MB$_2$ borides perform better, in the case of OER (Table 4) higher catalytic activities have been shown by the systems that include metal-rich borides, such as M_3B and M_2B (M = Fe, Co, Ni). Solid solutions of these borides have been also explored to optimize the catalytic performance. While the surface of such catalyst, quite obviously, undergoes substantial oxidation, as demonstrated by XPS and TEM measurements (97, 98), it is worth noting that they exhibit better performance than corresponding metals (99) or dispersed metal oxide NPs (98). These observations strongly support the hypothesis that the TMB core underlying the catalytically active shell enhances the overall stability and activity of such catalyst/precatalyst nanoheterostructure.

The layered structure of ternary boride, AlFe$_2$B$_2$ (Fig. 12), is similar to that of AlMoB, which was shown to exhibit an increased catalytic activity toward HER after the Al layers had been partially etched with NaOH solution. While AlFe$_2$B$_2$ dissolves rather quickly in acids (100), it is very stable in alkali solutions. Therefore, the Shatruk and Kolen'ko groups explored this material as a potential precatalyst for alkaline OER (98). The initial electrocatalytic cycles revealed a slight decrease in the η_{10} value, which stabilized at 240 mV after about 20 CV cycles and remained remarkably constant for ≈10 days. Examination of the catalyst after this activation period revealed that Al had been partially etched from the structure and a stable shell of catalytically active Fe$_3$O$_4$ NPs had been formed around the AlFe$_2$B$_2$ structure. Importantly, much poorer performance was observed when Fe$_3$O$_4$ NPs were used by themselves, without the underlying AlFe$_2$B$_2$ precatalyst.

Table 4. Selected examples of alkaline OER performance for TMB catalysts at pH = 14.

Compound	η_{10}, mV	b, mV dec^{-1}	Synthesis[a]	Ref.
AlFe$_2$B$_2$	240	42	Al + Fe + B, arc-melting; ball-milling	(98)
FeB	270	49	Fe + B, arc-melting; ball-milling	(98)
Co$_2$B	287	51	Co + B, ball-milling, 10 h	(101)
FeB$_2$	296	52	FeCl$_2$ + LiBH$_4$ in THF, 2 h at reflux; centrifugation; H$_2$O; 2 h at 873 K	(90)
Ni$_2$B	296	58	NiCl$_2$ + NaBH$_4$ + NaOH in H$_2$O/ethylenediamine, electrodeposition on Cu foil; 3 h at 473–573 K	(102)
Ni$_3$B	302	52	Ni(OAc)$_2$ + NaBH$_4$ + NaOH in H$_2$O, 10 min; centrifugation; H$_2$O/ethanol; 0.5–2.5 h at 623 K	(103)
Co$_3$B	≈370	n/a	CoBr$_2$ + LiBH$_4$ in THF, 2 h; filtration; 2 h at 773 K	(97)

[a] Sequential synthetic steps are separated by semicolons. See the cited articles for detailed synthetic procedures.
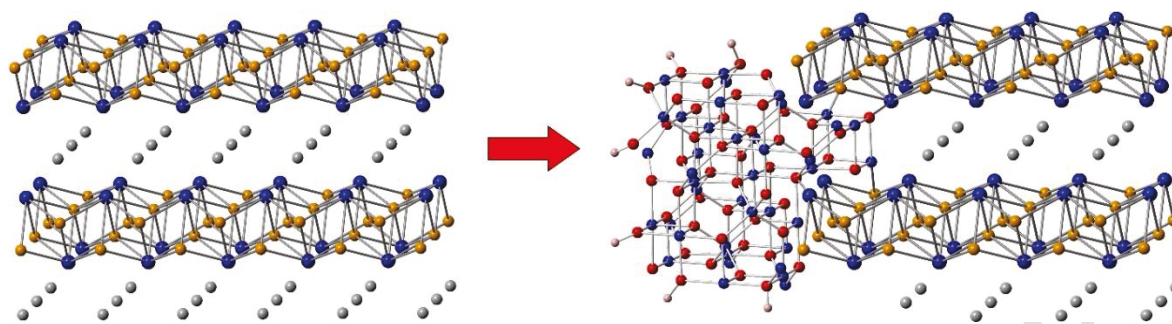
Fig. 12. The structure of $AlFe_2B_2$ (left) acts as a pre-catalyst toward OER electrolysis in alkaline solution. The initial activation is associated with the formation of the catalytically active layer of Fe_3O_4 on the surface of the pre-catalyst (right). Reproduced with permission from ref. (98).

8. Conclusions and outlook

Electrocatalysis is a rapidly evolving research area, and there are plenty of PGM-free catalysts reported in the literature, including Ni alloys, oxides, TMPs, and TMBs, as detailed here. Recent findings have shown that, while HER most likely takes place on the surface of the pristine Xide catalyst, the *in situ* formation of the real catalyst is clearly observed during OER as a result of surface oxidation of the Xides. Even though PGM-free Ni alloys, TMPs, and TMBs do not outperform Pt, their promising HER activity can be of practical importance due to significantly lower costs. In contrast, many Fe-, Co- and Ni-based catalysts outperform the standard IrO_2/RuO_2 oxides in OER activity, but little is known about the durability of these PGM-free materials. This is mainly due to the fact that the vast majority of the literature reports the results of laboratory half-cell measurements and the durability is only tested for a few weeks at most.

With respect to the synthesis, it is difficult to formulate the exact key requirements (*e.g.*, chemical composition, promoters, crystallographic/electronic/surface structures, physical properties, morphology, fine microstructure, specific surface area, particle size distribution, supporting material, *etc*.) that should be fulfilled for the HER/OER catalysts to be economic, active, stable and durable for AEMWE. This challenge is mainly explained by the ever increasing complexity of the reported catalysts, their dynamic reconstruction during reactions, and large scattering of the resultant half-cell testing data. The way to solve this shortcoming is to foster the international community working on water electrolysis to follow well-defined characterization and testing protocols. The recent efforts in this direction (30, 31) provide hope that the aforementioned requirements will be established in near-term, also involving the help of data mining and computation.It would be also interesting to see how Xides will compete and, more importantly, participate in the rapidly developing area of mass-efficient atomically dispersed catalysts for HER/OER (104, 105).

Considering the discovery of new, more efficient catalysts, solid-state chemistry offers a hundreds of ternary and multinary phosphides, borides, and other Xides, in addition to the relatively limited range of binary materials that have been studied thus far as potential HER/OER electrocatalysts. Such materials have unique crystal and electronic structures and may exhibit quite different catalytic properties as compared to their binary counterparts. Tuning the transition-metal *d*-orbital

filling, local metal and non-metal (B, C, N, Si, P, S, Se, Te) coordination environments, and the density of states at the Fermi level is important to optimizing the HER/OER catalytic performance. The large structural and compositional variety is a challenge as the synthesis and property characterization protocols are tedious. Application of computational/machine learning approaches can substantially accelerate identification of the most promising candidates. Coupling the computational screening, which accounts for surface dynamic, together with experimental research should result in emergent catalysts with improved performance.

Assembling even a single AEMWE cell is tedious process that requires expertise not commonly found in academic research laboratories. For instance, to the best of our knowledge, no full AEM electrolyzer has been tested with promising TMP/TMB cathodes and anodes. Nevertheless, real AEMWE testing is quite important to demonstrate the applied potential of Xides as catalysts. Here, the early involvement of the industry will be highly beneficial, allowing to understand the real future prospects of the reported PGM-free catalytic systems.

Another issue is the lack of benchmarked AEMWE components (membrane, ionomer, GDL, and PTL) and standard HER/OER catalysts accepted by the electrolyzer community. This state of matters makes comparison of performances not only difficult, but in many cases meaningless. Substantial input from academia, National Labs, and industry into standardization of materials and test protocols is needed. This work has been initiated in the international US–EU collaboration under the HydroGEN consortium (https://www.h2awsm.org) and has already resulted in the harmonization of testing protocols for PEMWE, which will be followed by expansion to the promising AEMWE field. Establishing such protocols will allow the electrolyzer community to work at the device level to engineer AEMWE electrolyzers with high performance and durability (16, 106).

Acknowledgments

References

(1) S.A. Sherif, F. Barbir, T.N. Veziroglu, *Electr. J.*, 2005, **18**, 62.
(2) A. Saeedmanesh, M.A. Mac Kinnon, J. Brouwer, *Curr. Opin. Electrochem.*, 2018, **12**, 166.
(3) T. Sinigaglia, F. Lewiski, M.E. Santos Martins, J.C. Mairesse Siluk, *Int. J. Hydrogen Energy*, 2017, **42**, 24597.
(4) A. Buttler, H. Spliethoff, *Renew. Sust. Energ. Rev.*, 2018, **82**, 2440.
(5) E. Pomerantseva, C. Resini, K. Kovnir, Y.V. Kolen'ko, *Adv. Phys. X*, 2017, **2**, 211.
(6) J. Brauns, T. Turek, *Processes*, 2020, **8**, 248.
(7) M. David, C. Ocampo-Martinez, R. Sanchez-Pena, *J. Energy Storage*, 2019, **23**, 392.
(8) J.B. Hansen, *Faraday Discuss.*, 2015, **182**, 9.

(9) A. Hauch, R. Küngas, P. Blennow, A.B. Hansen, J.B. Hansen, B.V. Mathiesen, M.B. Mogensen, *Science*, 2020, **370**, eaba6118.

(10) M. Carmo, D.L. Fritz, J. Mergel, D. Stolten, *Int. J. Hydrogen Energy*, 2013, **38**, 4901.

(11) J.R. Varcoe, P. Atanassov, D.R. Dekel, A.M. Herring, M.A. Hickner, P.A. Kohl, A.R. Kucernak, W.E. Mustain, K. Nijmeijer, K. Scott, T.W. Xu, L. Zhuang, *Energy Environ. Sci.*, 2014, **7**, 3135.

(12) I. Vincent, A. Kruger, D. Bessarabov, *Int. J. Hydrogen Energy*, 2017, **42**, 10752.

(13) K. Ayers, N. Danilovic, R. Ouimet, M. Carmo, B. Pivovar, M. Bornstein, *Annu. Rev. Chem. Biomol.*, 2019, **10**, 219.

(14) I. Vincent, D. Bessarabov, *Renew. Sust. Energ. Rev.*, 2018, **81**, 1690.

(15) W.E. Mustain, P.A. Kohl, *Nat. Energy*, 2020, **5**, 359.

(16) W.E. Mustain, M. Chatenet, M. Page, Y.S. Kim, *Energy Environ. Sci.*, 2020, **13**, 2805.

(17) A. Zhegur-Khais, F. Kubannek, U. Krewer, D.R. Dekel, *J. Membr. Sci.*, 2020, **612**, 118461.

(18) O. Schmidt, A. Gambhir, I. Staffell, A. Hawkes, J. Nelson, S. Few, *Int. J. Hydrogen Energy*, 2017, **42**, 30470.

(19) J.T. Fan, A.G. Wright, B. Britton, T. Weissbach, T.J.G. Skalski, J. Ward, T.J. Peckham, S. Holdcroft, *ACS Macro Lett.*, 2017, **6**, 1089.

(20) T. Nguyen, Z. Abdin, T. Holm, W. Merida, *Energy Convers. Manag.*, 2019, **200**, 112108.

(21) S.Z. Oener, M.J. Foster, S.W. Boettcher, *Science*, 2020, eaaz1487.

(22) T. Shinagawa, A.T. Garcia-Esparza, K. Takanabe, *Sci. Rep.*, 2015, **5**, 13801.

(23) M.T.M. Koper, *J. Electroanal. Chem.*, 2011, **660**, 254.

(24) J. Greeley, *Annu. Rev. Chem. Biomol. Eng.*, 2016, **7**, 605.

(25) J. Masa, W. Schuhmann, *J. Solid State Electrochem.*, 2020, **24**, 2181.

(26) J. Kibsgaard, I. Chorkendorff, *Nat. Energy*, 2019, **4**, 430.

(27) M.J. Craig, G. Coulter, E. Dolan, J. Soriano-López, E. Mates-Torres, W. Schmitt, M. García-Melchor, *Nat. Commun.*, 2019, **10**, 4993.

(28) C.C.L. McCrory, S. Jung, I.M. Ferrer, S.M. Chatman, J.C. Peters, T.F. Jaramillo, *J. Am. Chem. Soc.*, 2015, **137**, 4347.

(29) L.C. Seitz, C.F. Dickens, K. Nishio, Y. Hikita, J. Montoya, A. Doyle, C. Kirk, A. Vojvodic, H.Y. Hwang, J.K. Norskov, T.F. Jaramillo, *Science*, 2016, **353**, 1011.

(30) C. Wei, R.R. Rao, J. Peng, B. Huang, I.E.L. Stephens, M. Risch, Z.J. Xu, Y. Shao-Horn, *Adv. Mater.*, 2019, **31**, 1806296.

(31) D. Voiry, M. Chhowalla, Y. Gogotsi, N.A. Kotov, Y. Li, R.M. Penner, R.E. Schaak, P.S. Weiss, *ACS Nano*, 2018, **12**, 9635.

(32) S. Anantharaj, S.R. Ede, K. Karthick, S.S. Sankar, K. Sangeetha, P.E. Karthik, S. Kundu, *Energy Environ. Sci.*, 2018, **11**, 744.

(33) C. Wei, S.N. Sun, D. Mandler, X. Wang, S.Z. Qiao, Z.C.J. Xu, *Chem. Soc. Rev.*, 2019, **48**, 2518.

(34) S.N. Sun, H.Y. Li, Z.C.J. Xu, *Joule*, 2018, **2**, 1024.

(35) S. Jin, *ACS Energy Lett.*, 2017, **2**, 1937.

(36) B.R. Wygant, K. Kawashima, C.B. Mullins, *ACS Energy Lett.*, 2018, **3**, 2956.

(37) W. Li, D. Xiong, X. Gao, L. Liu, *Chem. Commun.*, 2019, **55**, 8744.

(38) L.K. Allerston, N.V. Rees, *Curr. Opin. Electrochem.*, 2018, **10**, 31.

(39) Y. Zhu, J. Wang, H. Chu, Y.-C. Chu, H.M. Chen, *ACS Energy Lett.*, 2020, **5**, 1281.

(40) Y. Zhang, L. Song, *ChemCatChem*, 2020, **12**, 3621.

(41) X. Peng, D. Kulkarni, Y. Huang, T.J. Omasta, B. Ng, Y. Zheng, L. Wang, J.M. LaManna, D.S. Hussey, J.R. Varcoe, I.V. Zenyuk, W.E. Mustain, *Nat Commun.*, 2020, **11**, 3561.

(42) J. Li, J. Gong, *Energy Environ. Sci.*, 2020, **13**, 3748.

(43) T. Asset, A. Roy, T. Sakamoto, M. Padilla, I. Matanovic, K. Artyushkova, A. Serov, F. Maillard, M. Chatenet, K. Asazawa, H. Tanaka, P. Atanassov, *Electrochim. Acta*, 2016, **215**, 420.

(44) C.A. Campos-Roldan, L. Calvillo, M. Boaro, R.D. Gonzalez-Huerta, G. Granozzi, N. Alonso-Vante, *ACS Appl. Energ. Mater.*, 2020, **3**, 4746.

(45) S. Kabir, K. Lemire, K. Artyushkova, A. Roy, M. Odgaard, D. Schlueter, A. Oshchepkov, A. Bonnefont, E. Savinova, D.C. Sabarirajan, P. Mandal, E.J. Crumlin, I.V. Zenyuk, P. Atanassov, A. Serov, *J. Mater. Chem. A*, 2017, **5**, 24433.

(46) A.N. Kuznetsov, A.A. Serov, *Eur. J. Inorg. Chem.*, 2016, **3**, 373.

(47) A.N. Kuznetsov, E.A. Stroganova, A.A. Serov, D.I. Kirdyankin, V.M. Novotortsev, *J. Alloy Compd.*, 2017, **696**, 413.

(48) D.G. Li, E.J. Park, W.L. Zhu, Q.R. Shi, Y. Zhou, H.Y. Tian, Y.H. Lin, A. Serov, B. Zulevi, E.D. Baca, C. Fujimoto, H.T. Chung, Y.S. Kim, *Nat. Energy*, 2020, **5**, 378.

(49) A. Roy, M.R. Talarposhti, S.J. Normile, I.V. Zenyuk, V. De Andrade, K. Artyushkova, A. Serov, P. Atanassov, *Sustain. Energy Fuels*, 2018, **2**, 2268.

(50) P. Shang, Z. Ye, Y. Ding, Z. Zhu, X. Peng, G. Ma, D. Li, *ACS Sustain. Chem. Eng.*, 2020, **8**, 10664.

(51) A. Zadick, L. Dubau, K. Artyushkova, A. Serov, P. Atanassov, M. Chatenet, *Nano Energy*, 2017, **37**, 248.

(52) N.I. Andersen, A. Serov, P. Atanassov, *Appl. Catal. B Environ.*, 2015, **163**, 623.

(53) W.-S. Choi, M.J. Jang, Y.S. Park, K.H. Lee, J.Y. Lee, M.-H. Seo, S.M. Choi, *ACS App. Mater. Interfaces*, 2018, **10**, 38663.

(54) E. Cossar, A.O. Barnett, F. Seland, E.A. Baranova, *Catalysts*, 2019, **9**, 814.

(55) H. Koshikawa, H. Murase, T. Hayashi, K. Nakajima, H. Mashiko, S. Shiraishi, Y. Tsuji, *ACS Catal.*, 2020, **10**, 1886.

(56) E. Lopez-Fernandez, J. Gil-Rostra, J.P. Espinos, A.R. Gonzalez-Elipe, F. Yubero, A. de Lucas-Consuegra, *J. Power Sources*, 2019, **415**, 136.

(57) C.C. Pavel, F. Cecconi, C. Emiliani, S. Santiccioli, A. Scaffidi, S. Catanorchi, M. Comotti, *Angew. Chem. Int. Ed.*, 2014, **53**, 1378.

(58) A. Serov, N.I. Andersen, A.J. Roy, I. Matanovic, K. Artyushkova, P. Atanassov, *J. Electrochem. Soc.*, 2015, **162**, F449.

(59) H.A. Firouzjaie, W.E. Mustain, *ACS Catal.*, 2020, **10**, 225.

(60) M.A. Shaun, S.R. Kimberly, S.B. Jefferey, C. David, *J. Electrochem. Soc.*, 2020, **167**, 144512.

(61) D. Li, H. Liu, L. Feng, *Energy Fuels*, 2020, **34**, 13491.

(62) H. Chen, X. Liang, Y. Liu, X. Ai, T. Asefa, X. Zou, *Adv. Mater.*, 2020, **32**, 2002435.

(63) X. Bo, R.K. Hocking, S. Zhou, Y. Li, X. Chen, J. Zhuang, Y. Du, C. Zhao, *Energy Environ. Sci.*, 2020, **13**, 4225.

(64) D.Y. Chung, P.P. Lopes, P. Farinazzo Bergamo Dias Martins, H. He, T. Kawaguchi, P. Zapol, H. You, D. Tripkovic, D. Strmcnik, Y. Zhu, S. Seifert, S. Lee, V.R. Stamenkovic, N.M. Markovic, *Nat. Energy*, 2020, **5**, 222.

(65) Y. Liu, X. Liang, L. Gu, Y. Zhang, G.-D. Li, X. Zou, J.-S. Chen, *Nat. Commun*, 2018, **9**, 2609.

(66) K.N. Dinh, Q. Liang, C.-F. Du, J. Zhao, A.I.Y. Tok, H. Mao, Q. Yan, *Nano Today*, 2019, **25**, 99.

(67) Y. Sun, T. Zhang, C. Li, K. Xu, Y. Li, *J. Mater. Chem. A*, 2020, **8**, 13415.

(68) B. Owens-Baird, J.Y. Xu, D.Y. Petrovykh, O. Bondarchuk, Y. Ziouani, N. Gonzalez-Ballesteros, P. Yox, F.M. Sapountzi, H. Niemantsverdriet, Y.V. Kolen'ko, K. Kovnir, *Chem. Mater.*, 2019, **31**, 3407.

(69) B. Owens-Baird, Y.V. Kolen'ko, K. Kovnir, *Chem.Eur. J.*, 2018, **24**, 7298.

(70) J. Zhu, L. Hu, P. Zhao, L.Y.S. Lee, K.-Y. Wong, *Chem. Rev.*, 2020, **120**, 851.

(71) X.G. Wang, Y.V. Kolen'ko, X.Q. Bao, K. Kovnir, L.F. Liu, *Angew. Chem. Int. Ed.*, 2015, **54**, 8188.

(72) J.D. Costa, J.L. Lado, E. Carbó-Argibay, E. Paz, J. Gallo, M.F. Cerqueira, C. Rodríguez-Abreu, K. Kovnir, Y.V. Kolen'ko, *J. Phys. Chem. C*, 2016, **120**, 16537.

(73) B. Owens-Baird, J.P.S. Sousa, Y. Ziouani, D.Y. Petrovykh, N. Zarkevich, D.D. Johnson, Y.V. Kolen'ko, K. Kovnir, *Chem. Sci.*, 2020, **11**, 5007.

(74) F.M. Sapountzi, E.D. Orlova, J.P.S. Sousa, L.M. Salonen, O.I. Lebedev, G. Zafeiropoulos, M.N. Tsampas, H.J.W. Niemantsverdriet, Y.V. Kolen'ko, *Energy Fuels*, 2020, **34**, 6423.

(75) L.A. King, M.A. Hubert, C. Capuano, J. Manco, N. Danilovic, E. Valle, T.R. Hellstern, K. Ayers, T.F. Jaramillo, *Nat. Nanotechnol*, 2019, **14**, 1071.

(76) H. Kim, J. Kim, S.K. Kim, S.H. Ahn, *Appl. Catal. B Environ.*, 2018, **232**, 93.

(77) J.W.D. Ng, T.R. Hellstern, J. Kibsgaard, A.C. Hinckley, J.D. Benck, T.F. Jaramillo, *ChemSusChem*, 2015, **8**, 3512.

(78) J.Y. Xu, X.K. Wei, J.D. Costa, J.L. Lado, B. Owens-Baird, L.P.L. Goncalves, S.P.S. Fernandes, M. Heggen, D.Y. Petrovykh, R.E. Dunin-Borkowski, K. Kovnir, Y.V. Kolen'ko, *ACS Catal.*, 2017, **7**, 5450.

(79) J.Y. Xu, J.P.S. Sousa, N.E. Mordvinova, J.D. Costa, D.Y. Petrovykh, K. Kovnir, O.I. Lebedev, Y.V. Kolen'ko, *ACS Catal.*, 2018, **8**, 2595.

(80) J.L. Lado, X.G. Wang, E. Paz, E. Carbo-Argibay, N. Guldris, C. Rodriguez-Abreu, L.F. Liu, K. Kovnir, Y.V. Kolen'ko, *ACS Catal.*, 2015, **5**, 6503.

(81) T.E. Rosser, J.P.S. Sousa, Y. Ziouani, O. Bondarchuk, D.Y. Petrovykh, X.K. Wei, J.J.L. Humphrey, M. Heggen, Y.V. Kolen'ko, A.J. Wain, *Catal. Sci. Technol.*, 2020, **10**, 2398.

(82) G. Akopov, M.T. Yeung, R.B. Kaner, *Adv. Mater.*, 2017, **29**, 1604506.

(83) M. Shatruk, Chemical aspects of itinerant magnetism, in: R.A. Scott (Ed.), Encyclopedia of Inorganic and Bioinorganic Chemistry, Wiley-VCH, Chichester, 2017, p. DOI: 10.1002/9781119951438.eibc2494.

(84) F.A. Garcés-Pineda, M. Blasco-Ahicart, D. Nieto-Castro, N. López, J.R. Galán-Mascarós, *Nat. Energy*, 2019, **4**, 519.

(85) E. Westsson, S. Picken, G. Koper, *Front. Chem.*, 2020, **8**, 163.

(86) Y. Sun, J. Wang, Q. Liu, M. Xia, Y. Tang, F. Gao, Y. Hou, J. Tse, Y. Zhao, *J. Mater. Chem. A*, 2019, **7**, 27175.

(87) M.J. Hülsey, C.W. Lim, N. Yan, *Chem. Sci.*, 2020, **11**, 1456.

(88) X. Zou, L. Wang, X. Ai, H. Chen, X. Zou, *Chem. Commun.*, 2020, **56**, 3061.

(89) Y. Chen, G. Yu, W. Chen, Y. Liu, G.-D. Li, P. Zhu, Q. Tao, Q. Li, J. Liu, X. Shen, H. Li, X. Huang, D. Wang, T. Asefa, X. Zou, *J. Am. Chem. Soc.*, 2017, **139**, 12370.

(90) H. Li, P. Wen, Q. Li, C. Dun, J. Xing, C. Lu, S. Adhikari, L. Jiang, D.L. Carroll, S.M. Geyer, *Adv. Energy Mater.*, 2017, **7**, 1700513.

(91) P.R. Jothi, Y. Zhang, K. Yubuta, D.B. Culver, M. Conley, B.P.T. Fokwa, *ACS Appl. Energy Mater.*, 2019, **2**, 176.

(92) Q. Li, X. Zou, X. Ai, H. Chen, L. Sun, X. Zou, *Adv. Energy Mater.*, 2019, **9**, 1803369.

(93) H. Vrubel, X. Hu, *Angew. Chem. Int. Ed.*, 2012, **51**, 12703.

(94) H. Park, A. Encinas, J.P. Scheifers, Y. Zhang, B.P.T. Fokwa, *Angew. Chem. Int. Ed.*, 2017, **56**, 5575.

(95) Y. Jiang, Y. Lu, *Nanoscale*, 2020, **12**, 9327.

(96) L.T. Alameda, C.F. Holder, J.L. Fenton, R.E. Schaak, *Chem. Mater.*, 2017, **29**, 8953.

(97) A.-M. Zieschang, J.D. Bocarsly, J. Schuch, C.V. Reichel, B. Kaiser, W. Jaegermann, R. Seshadri, B. Albert, *Inorg. Chem.*, 2019, **58**, 16609.

(98) D.K. Mann, J. Xu, N.E. Mordvinova, V. Yannello, Y. Ziouani, N. González-Ballesteros, J.P.S. Sousa, O.I. Lebedev, Y.V. Kolen'ko, M. Shatruk, *Chem. Sci.*, 2019, **10**, 2796.

(99) F. Guo, Y. Wu, H. Chen, Y. Liu, L. Yang, X. Ai, X. Zou, *Energy Environ. Sci.*, 2019, **12**, 684.

(100) X. Tan, P. Chai, C.M. Thompson, M. Shatruk, *J. Am. Chem. Soc.*, 2013, **135**, 9553.

(101) X. Ma, J. Wen, S. Zhang, H. Yuan, K. Li, F. Yan, X. Zhang, Y. Chen, *ACS Sust. Chem. Eng.*, 2017, **5**, 10266.

(102) J. Jiang, M. Wang, W. Yan, X. Liu, J. Liu, J. Yang, L. Sun, *Nano Energy*, 2017, **38**, 175.

(103) W.-J. Jiang, S. Niu, T. Tang, Q.-H. Zhang, X.-Z. Liu, Y. Zhang, Y.-Y. Chen, J.-H. Li, L. Gu, L.-J. Wan, J.-S. Hu, *Angew. Chem. Int. Ed.*, 2017, **56**, 6572.

(104) Y. Yang, Y. Yang, Z. Pei, K.-H. Wu, C. Tan, H. Wang, L. Wei, A. Mahmood, C. Yan, J. Dong, S. Zhao, Y. Chen, *Matter*, 2020, **3**, 1442.

(105) Y. Wang, H. Su, Y. He, L. Li, S. Zhu, H. Shen, P. Xie, X. Fu, G. Zhou, C. Feng, D. Zhao, F. Xiao, X. Zhu, Y. Zeng, M. Shao, S. Chen, G. Wu, J. Zeng, C. Wang, *Chem. Rev.*, 2020, **120**, 12217.

(106) N. Ul Hassan, M. Mandal, G. Huang, H.A. Firouzjaie, P.A. Kohl, W.E. Mustain, *Adv. Energy Mater.*, 2020, **10**, 2001986.

The Authors

	Alexey is a Chief Scientist in Pajarito Powder, US-based company manufacturing electrocatalysts for fuel cells and electrolyzers. He has more than 10 years of industrial experience in the design, synthesis and manufacturing of new energy-related materials.
	Kirill is an Associate Professor of Chemistry at Iowa State University and Research Scientist at US DOE Ames Laboratory. He enjoyed solid state chemistry research starting from freshman year at Moscow State University. Kirill's research interests are in the broad field of solid-state and materials chemistry with special focus on the development of unconventional synthetic routes towards novel inorganic solids; prediction, synthesis, and structural characterization of complex pnictides, tetrelides, and borides; and development of novel thermoelectric, magnetic, catalytic, and non-linear optical materials.
	Michael is interested in applications of intermetallic materials to problems of catalysis and magnetism. His fascination with the structures and properties of intermetallics nucleated during graduate studies at Lomonosov Moscow State University and a postdoctoral stint at Cornell University. He continues to explore and share this passion as professor of inorganic and materials chemistry at Florida State University.
	Yury enjoys synthesis, investigation & application of unconventional nanomaterials. Particular emphasis is placed on catalysis, clean energy technology, and multifunctional coatings. He is happy to collaborate on these topics with his university friends Alexey, Kirill and Michael.